Chitosan-hydroxypropyl methylcellulose tioconazole films: A promising alternative dosage form for the treatment of vaginal candidiasis

Natalia L. Calvo, Laura A. Svetaz, Vera A. Alvarez, Ariel D. Quiroga, María C. Lamas, Darío Leonardi

PII: S0378-5173(18)30917-7
DOI: https://doi.org/10.1016/j.ijpharm.2018.12.011
Reference: IJP 17980

To appear in: *International Journal of Pharmaceutics*

Received Date: 17 September 2018
Revised Date: 30 November 2018
Accepted Date: 4 December 2018

Please cite this article as: N.L. Calvo, L.A. Svetaz, V.A. Alvarez, A.D. Quiroga, M.C. Lamas, D. Leonardi, Chitosan-hydroxypropyl methylcellulose tioconazole films: A promising alternative dosage form for the treatment of vaginal candidiasis, *International Journal of Pharmaceutics* (2018), doi: https://doi.org/10.1016/j.ijpharm.2018.12.011

Chitosan-hydroxypropyl methylcellulose tioconazole films: A promising alternative dosage form for the treatment of vaginal candidiasis

Natalia L. Calvo[a,b], Laura A. Svetaz[c], Vera A. Alvarez[d], Ariel D. Quiroga[e,f], María C. Lamas [a,g,*], Darío Leonardi [a,g,*]

[a]Instituto de Química Rosario (IQUIR, CONICET-UNR), Suipacha 531, Rosario (S2002LRK), Argentina.

[b]Área Análisis de Medicamentos, Facultad de Ciencias Bioquímicas y Farmacéuticas, Universidad Nacional de Rosario, Suipacha 531, Rosario (S2002LRK), Argentina.

[c]Área Farmacognosia, Facultad de Ciencias Bioquímicas y Farmacéuticas, Universidad Nacional de Rosario, Suipacha 531, Rosario (S2002LRK), Argentina.

[d]Grupo de Materiales Compuestos Termoplásticos (CoMP), Instituto de Investigaciones de Ciencia y Tecnología de Materiales (INTEMA, CONICET-UNMdP), Colón 10890, Mar del Plata (7600), Argentina.

[e]Instituto de Fisiología Experimental (IFISE, CONICET-UNR), Suipacha 531, Rosario (S2002LRK), Argentina.

[f]Área Morfología, Facultad de Ciencias Bioquímicas y Farmacéuticas, Universidad Nacional de Rosario, Suipacha 531, Rosario (S2002LRK), Argentina.

[g]Área Técnica Farmacéutica, Facultad de Ciencias Bioquímicas y Farmacéuticas, Universidad Nacional de Rosario, Suipacha 531, Rosario (S2002LRK), Argentina.

Corresponding authors

Phone: 54-341-4804592. FAX: 54-341-4370477. Facultad de Ciencias Bioquímicas y Farmacéuticas, Universidad Nacional de Rosario, Suipacha 531, 24 (2000) Rosario, Argentina.

E-mail addresses: leonardi@iquir-conicet.gov.ar (D. Leonardi), mlamas@fbioyf.unr.edu.ar (M. Lamas)

Abstract

Vaginal candidiasis is considered a frequent opportunistic mucosal infection and the second most common cause of vaginitis after bacterial vaginosis. In this work, different vaginal films based on chitosan, hydroxypropyl methylcellulose and blends of these polymers containing tioconazole, were developed and thoroughly characterized to improve the conventional therapeutics of vaginal candidiasis. Mechanical properties, swelling, adhesiveness, morphology, antifungal activity, hemocompatibility and cytotoxicity were evaluated. The drug solid state in the films was analyzed by thermal and X-ray diffraction analysis. Films showed homogeneous surfaces and presented similar mechanical properties and adhesiveness. Time-kill studies displayed that films were more active than both tioconazole pure drug and traditional tioconazole ovule against *Candida albicans*, which is probably related to the fact that tioconazole is in amorphous state inside the films. Although all formulations proved to be hemocompatible, films based only on chitosan exhibited a certain degree of cytotoxicity and therefore they should be avoided. The system based on chitosan-hydroxypropyl methylcellulose with 40% PEG 400 as plasticizer presented fast antimicrobial activity as well as the lowest swelling. Additionally, this formulation did not produce substantial hemolytic and cytotoxic effects, indicating that films based on chitosan-hydroxypropyl methylcellulose could be a promising alternative dosage form for the treatment of vaginal candidiasis.

Keywords: Vaginal candidiasis; Films; Mechanical properties; Antifungal activity; Cytotoxicity

1. Introduction

Vaginal candidiasis is considered a frequent opportunistic mucosal infection in women, being the second most common cause of vaginitis after bacterial vaginosis (Egan and Lipsky, 2000). The disease affects 70 - 75% women at least once in their lifetime and around 50% of patients experience a recurrence (Costa-de-Oliveira et al., 2008). Although different Candida species may produce this disease, *Candida albicans* is the most prevalent yeast causing this infection. Vaginal candidiasis is commonly treated using azole antifungals, such as fluconazole, miconazole, itraconazole, clotrimazole, econazole, ketoconazole and tioconazole (Bassi and Kaur, 2015). Tioconazole (TCZ, (1[2-(2-chloro-3-thienyl) methoxy-2-(2,4-dichlorro-phenyl)ethyl]-H-imidazole) is an imidazole antifungal agent with a broad spectrum of activity against a variety of microorganisms (Carrillo-Muñoz et al., 2010). This drug has been shown to hold higher activity against *C. albicans* than clotrimazole, econazole, ketoconazole and miconazole (Lefler and Stevens, 1984). This could be due to the fact that TCZ possesses antifungal activity even when yeast cells are in the stationary phase, while common antifungal agents such as ketoconazole and micronazole display with antimicrobial activity only when yeasts are in the growth phase (Beggs, 1984).

The effectiveness of a treatment is not only determined by the antifungal compound type, but also by the development of an adequate dosage form, which is determinant in the biological activity of a therapeutic system. Particularly, pharmaceutical dosage forms for local vaginal delivery need to remain in the site of infection as long as possible and to be able to release the active compound according to the treatment. The use of conventional vaginal formulations such as creams, gels, pessaries, and foams is discouraged due to their poor retention in the vaginal tract by the tract's self-cleansing action (Alam et al., 2007). Other conventional formulations such as vaginal tablets and ovules show good retention abilities, but both are rigid and may produce discomfort. Alternative bioadhesive vaginal formulations

such as films are suitable forms to achieve effective drug release for extended periods of time (Cautela et al., 2018; Ghosal et al., 2014; Machado et al., 2016; Mishra et al., 2017; Srinivasan et al., 2016; Traore et al., 2018; Yoo et al., 2009). In addition, these films present more flexibility than tablets and ovules, which may improve patients' compliance.

Several biocompatible polymers such as chitosan (CH) and hydroxypropyl methyl cellulose (HPMC) have been employed to develop mucoadhesive films. CH, a cationic natural polymer widely used in pharmaceutical applications shows attractive biological properties including biocompatibility, biodegradability, non-toxicity, and physiological inertness (Krajewska, 2004). HPMC, a non ionic polymer, is a semi-synthetic cellulose derivative usually employed in the pharmaceutical industry, mainly as gelling agent and to control the release of pharmaceutical drugs (Kamel et al., 2008; Saha and Bhattacharya, 2010).

The aim of this work was to develop and thoroughly characterize novel TCZ film dosage forms in order to improve the therapeutics of vaginal candidiasis. TCZ films were compared with the TCZ ovule, which is the traditional dosage form selected to treat the infectious disease.

2. Materials and Methods

2.1. Chemicals

TCZ raw material of pharmaceutical grade (BP 2002) and PEG 400 were acquired in Saporiti (Buenos Aires, Argentina). During the experiments, the drug was kept in a desiccator. Double-distilled water was used for the preparation of aqueous solutions. TCZ vaginal ovule ("Honguil" from Raymos laboratories) containing 0.30 g TCZ and excipients [liquid vaseline (0.45 g) and solid vaseline (1.35 g)] was acquired in a local Drugstore (Rosario, Argentina). CH (230 KDa average molecular weight and 80.6% of N-deacetylation) was supplied by Aldrich Chemical Co. (Milwaukee, WI, USA). HPMC (MW 250 kDa, methoxyl content 19-

24%, hydroxypropyl content 7-12%) was purchased from Eigenman & Veronelli (Milan, Italy). All other chemicals were of analytical grade.

2.2. Methods

2.2.1. Film preparation

Films were prepared by solvent evaporation. CH solution (1% w/v) was obtained dispersing CH in 1% v/v lactic acid (v/v). TCZ was suspended in PEG 400 used as plasticizer and added to the CH solution. Aqueous solution of HPMC (1% w/v) was prepared and stirred overnight. Then, CH solution was dripped over HPMC solution at 40 °C to avoid precipitation and stirred at 200 rpm (Boecco stirrer, Germany) for 1 h. Finally, the solutions were cast on 10 cm diameter Petri dishes and dried at 40 ºC. Unloaded films were developed following the same procedure but without adding TCZ to the mixtures, B1 consisted of 0.25:0.75 (CH:HPMC) ratio and B2 1:0 (CH:HPMC) ratio. Dried films were removed from the Petri dishes and conditioned in a chamber at 25 °C and 80% RH for 24 h.

Table 1. Composition of loaded films.

Film	CH 1% w/v	HPMC 1% w/v	PEG (% w/w)	TCZ (% w/w)
S1	0.25	0.75	5	15
S2	1	-	5	15
S3	0.25	0.75	40	15
S4	1	-	40	15

2.2.2. Film Characterization

2.2.2.1. Thickness (TH) and folding endurance (FE)

For each system, six thickness measurements were made (around and in the center of

the films) with a digital micrometer (Schwyz, China). Folding endurance was determined by repeatedly folding the films at the same place until they broke or were folded 300 times (meeting the assay) (Avachat et al., 2013).

2.2.2.2. Mechanical properties: Load at break (LB) and Elongation at Break (EB)

The mechanical strength of the films was evaluated by using an Instron universal testing machine, EMIC 2350 (Instron, Norwood, MA, USA) with a 50 N load cell. Films for each mechanical test were conditioned (at 25 °C and 75% RH for 24 h) and cut into strips (7 mm wide and 60 mm long) to evaluate tensile properties. The initial grip distance was 30 mm and the crosshead speed was 5.0 mm/min. The parameters obtained from stress/strain curves were load at break (maximum force at breaking), and elongation (calculated as the percentile of the change in the length of film with respect to the original distance between the grips). For each mechanical probe, three replicate measurements were performed.

2.2.2.3. *In vitro* mucoadhesive strength (MS)

An Instron universal testing machine, EMIC 2350 (Instron, Norwood, MA, USA) with a 50 N load cell was employed to analyze the mucoadhesive strength of each film. The force required to detach each formulation from a disc of porcine vaginal mucosa (obtained from "Paladini" slaughterhouse, V.G. Galvez, Argentina) was measured. A portion of each film (2.5 cm diameter) was added to the upper end of the cylindrical probe and gum discs (obtained by punch biopsy and hydrated with 0.5 mL artificial vaginal fluid for 2 min) were horizontally attached to the lower end of the cylindrical probe by using double-sided adhesive tape (Tejada et al., 2018b). Simulated vaginal fluid pH value 4.2 (composed by (g L^{-1}): NaCl, 3.51; KOH, 1.40; $Ca(OH)_2$, 0.222; bovine serum albumin, 0.018; lactic acid, 2.00; acetic acid,

1.00; glycerol, 0.160; urea, 0.400 and glucose, 5.00) was prepared according to previous literature (Owen and Katz, 1999).

Each film remained in contact with the gum for 1 min and it was then moved upwards at a constant speed (1.0 mm/min). The test was carried out in triplicate. The force required to detach each film from the gum disc was determined from the resulting force/time plot.

2.2.2.4. Swelling index (SI)

Swelling measurements were determined by immersing an accurately weighted portion of the films (around 50 mg) in 0.5 mL simulated vaginal fluid at 37 ºC.

Films were carefully removed at predetermined time intervals (0, 5, 10, 15, 20, 30, 45, 60, 90, 120, 150, 180, 210, and 240 min), and the excess adhering moisture was gently blotted off, and weighed. Then, 0.5 mL of simulated vaginal fluid was added again. The swelling index was calculated using the weights of dried (*Wo*) and swollen (*Ws*) films (Eq. (1)). The test was carried out in triplicate.

$$SI: \quad \frac{Ws - Wo}{Wo} \qquad \text{(Eq. 1)}$$

2.2.2.5. Fourier transformed infrared spectroscopy (FTIR)

Infrared (IR) spectra were acquired in a Shimadzu Prestige 21 spectrometer (Shimadzu Corp., Kyoto, Japan) over a wave number range of 4000-600 cm^{-1}. ATR (attenuated total reflectance) experiments were carried out with a diamond-based ATR accessory (GladiATR, Pike Technologies, Madison, USA) fitted with a Pike temperature control unit. An average of 20 scans was used at a 4 cm^{-1} resolution between 4000 and 600 cm^{-1} in all cases. The temperature (30 ºC), the amount of sample, and the pressure exerted on the sample during the

186 measurement were standardized. Each system was scanned three times and the measurements
187 averaged.
188
189 2.2.2.6. Thermal analysis
190 Calorimetric determinations were performed in a Linseis PT1000 differential scanning
191 calorimeter (DSC, Linseis Inc., New Jersey, USA), operating under a constant nitrogen flow
192 (8 mL/min). Each sample, 2 mg (TCZ) or 5-6 mg (ovule and films), was placed in closed
193 aluminum pans perforated with a pin-hole to equilibrate pressure from the potential expansion
194 of evolved gases or residual solvents, and heated from 40 to 145 ºC at 10 ºC/min. An empty
195 pan was used as a reference.
196 Thermogravimetric analysis (TGA) tests were carried out using a thermal analyzer
197 (Model TGA Q500, Hüllhorst, Germany). Samples (around 8 mg) were heated at a constant
198 rate of 10 °C/min from room temperature up to 600 °C under a nitrogen flow of 30 mL/min in
199 order to avoid thermo oxidative reactions.
200
201 2.2.2.7. X-ray diffraction analysis (XRD)
202 X-ray diffractograms were obtained with a PAN analytical X'Pert PRO diffractometer
203 (Netherlands) equipped with a monochromatic CuK_{α} radiation source (λ = 1.5406 Å)
204 operating at a voltage of 40 kV and current 40 mA at a scanning rate of 0.02 º per sec. The
205 scanning region was in a 2θ range from 5 ° to 40 °.
206
207 2.2.2.8. Scanning electron microscopy (SEM)
208 The morphology of films was investigated by scanning electron microscopy (SEM,
209 AMR 1000, Leitz, Wetzlar, Germany). Samples were mounted on an aluminum support using
210 conductive, double-sided adhesive tape, and coated with a fine gold layer for 15 min at 70–80

mTorr in order to make them conductive before obtaining the SEM micrographs. All samples were examined using an accelerating voltage of 20 kV and magnifications of 200x, 1000x and 5000x (Priotti et al., 2017).

2.2.2.9. Dissolution Studies

Dissolution studies were performed in 900 mL of distilled water (pH 4.3 mimic to the vaginal tract) at 37°C, using a USP XXIV Apparatus 2 (Paddle Apparatus) (Hanson Research, SR8 8-Flask Bath, Ontario, Canada) with paddles rotating at 50 rpm (Pharmacopoeia, 2017; Tejada et al., 2018b). TCZ raw material (135 mg) was dispersed in the dissolution medium. Films (containing 135 mg TCZ) were fixed to the central shaft using cyanoacrylate adhesive (Pharmacopoeia, 2017; Shaker et al., 2018; Tejada et al., 2017b). At different time intervals: 0, 5, 15, 30, 45, 60, 90, 120, 180, 240, and 360 min, aliquot of 5 mL each were taken (without replacement) using a 0.45 µm filter. The amount of dissolved TCZ was determined by spectroscopic measures at 225 nm using an Agilent 8453 UV–DAD spectrophotometer (Agilent Technologies, Santa Clara, USA). Determinations were performed in a quartz cell (10 mm optical path length) against a blank of dissolution media. The assay was carried out in triplicate.

2.2.2.10. Biological Activity of loaded and unloaded films

2.2.2.10.1. Halo zone test over time

Halo zone test was performed following the guidelines of the disc diffusion method described in CLSI document M44-A2 [36]. *C. albicans* (ATCC 10231) was cultured in Sabouraud's dextrose agar 24 h before testing. Testing was carried out on agar plates (150 mm diameter) containing Mueller-Hinton agar, supplemented with 2% glucose (2 g/100 mL) and 0.5 µm/mL methylene blue, at a depth of 4.0 mm. The inoculants were prepared by

suspending five distinct colonies in 5 mL of sterile distilled water and shaking on a vortex mixer for 15 s. The agar surface was inoculated by dipping sterile cotton swabs into a cell suspension adjusted to a turbidity of a 0.5 McFarland standard (approximately 1 – 5 x10^6 CFU/mL) and by streaking the plate surface in three directions. The plate was allowed to dry for 20 min, then the TCZ powder (0.34 mg), used as control, was placed attached to a Scotch tape onto the agar surface. Additionally, ovule content (mass equivalent to 0.34 mg TCZ) was embedded in a paper disc and placed onto the agar surface. Each film, paper disc, and Scotch tape was moved to another area of the culture after 2, 4, 6, 8, 10, 24, 48, 72, and 96 h (4 days). After that, the plates were incubated in air at 28°C and read after 24 h. Halo diameters (in millimeters) for the zone of complete inhibition were determined using a caliper, and the mean value was recorded (Tejada et al., 2018a).

2.2.2.10.2. Time-kill

C. albicans ATCC 10231 was cultured in Sabouraud dextrose agar (SDA) 24 h before testing. The inoculum was prepared by suspending five distinct colonies in sterile distilled water and shaking on a vortex mixer for 15 s. Cell suspension was adjusted to the turbidity of a 0.5 McFarland standard (approximately 1– 5x10^6 CFU/mL). TCZ (0.34 mg), ovule (2.38 mg equivalent to 0.34 mg TCZ) and films (disc with a diameter of 5 mm equivalent to 0.34 mg TCZ) were placed in 5 mL of inoculum. The suspensions were mixed for 20 s with a vortex mixer, and samples (0.05 mL) were taken at 0, 30, 60, 90, 120, 150, 180, 210, 240 and 360 min, and serially diluted before spreading onto SDA. The plates were incubated for 24 h and the viable colonies were evaluated. The time-kill curves (Cantón et al., 2009) were constructed by plotting the CFU/mL surviving at each time point in the presence and absence of the formulations. Experiments were conducted in triplicate and the mean number of survivors was determined.

2.2.2.11. Cytotoxicity of loaded and unloaded films

2.2.2.11.1. Extraction assay from films

To achieve the extraction of the film components, discs (5 mm diameter) were placed in the sidewalls of a 12 well plate and Dulbecco's modified Eagle's medium (DMEN , 1200 µL) was added to each well and incubated at 37 ºC for 12-16 h. Then, the media were used for the analysis of cellular metabolic activity by MTT assay.

2.2.2.11.2. Cytotoxicity

Human HCC cell lines Huh7 were obtained from JCRB Cell Bank (Tokyo, Japan). The top priority of this assay was to measure cell damage by the drugs. The use of different cell lines other than vaginal-derived cells was considered as a proper system since we did not mean to measure any hepatic effects; rather, we measured cytotoxicity of the drugs and their combinations with polymers. Allen et al. reported that cell lines tend to exhibit problems in stability and/or viability, and because of this, they do not always prove to be the ideal system. Thus, the use of cell lines able to overcome these limitations, such as those derived from other tissues, is recommended as a feasible alternative, especially regarding new potential applications in drug testing therapy (Allen et al., 2005). Cells were maintained in Dulbecco's modified Eagle's medium (DMEM) supplemented with 10% fetal bovine serum, 100 IU/mL penicillin, and 100 µg/mL streptomycin at 37 °C in a humidified atmosphere of 95% O_2 and 5% CO_2. In all experiments, cells were treated after 24 h of attachment with 200 µL extraction media. Control (untreated) cells were incubated without TCZ.

2.2.2.11.3. MTT assay

Cells were seeded in 96-well plates at a density of 3500 cells/well. After 24 h of attachment, cells were treated for 24 h with the different extraction media obtained in section

2.2.2.10.1. After treatment, 3-(4,5-dimethyl-2-thiazolyl)-2,5-diphenyl-2H-tetrazolium bromide (MTT; Sigma-Aldrich Corp.) was added into the culture medium to assess its metabolization, as previously described (Ferretti et al., 2016). Absorbance of the metabolite produced from viable cells was detected at 540 nm (reference filter 650 nm) in a DTX 880 multimode detector (Beckman Coulter Inc., Fullerton, CA, USA). Results were expressed as percentage of absorbance in control cells.

2.2.1.12. Statistical analysis and graphics software

Analysis of variance was used, and when the effect of the factors was significant, the Tukey multiple ranks honestly significant difference test was applied (Origin 8.5, OriginLabCo., Northampton, USA). Differences at $p < 0.01$ were considered significant.

3. Results and discussion

3.1. Mechanical properties

Loaded and unloaded films were uniform in texture. The thickness (Figure 1A) was found to range from 0.197 ± 0.064 to 0.297 ± 0.033 mm, which was significantly smaller than the ovule (25x10x10 mm). Therefore, the films could produce lesser discomfort after application than the ovule. It should be mentioned that the thickness of the films was even smaller than that obtained by Dobaria et al. They developed itraconazole bioadhesive vaginal films and considered as the optimal formulation a film with a thickness of 0.46 mm (Dobaria et al., 2009). Folding endurance was performed in order to evaluate film flexibility to produce a secure application. Prepared films were folded 300 times without breaking, meeting the folding endurance test (Avachat et al., 2013). The elongation value (Figure 1B) of film S4 (based on CH and 40 % w/w PEG 400) was the highest ($p < 0.01$). This fact could be explained by the combination of both high CH concentration and high percentage of

plasticizer. This result is in agreement with that previously obtained by Suyatma et al. (Suyatma et al., 2005), where the highest elongation for CH films was obtained when PEG 400 at 40% was used as plasticizer. Also, when comparing formulations S3 and S4, it can be noted that a high HPMC ratio (0.75) produces a decrease in the elasticity values of the films. These results are in agreement with those obtained by Tejada et al., indicating a remarkable reduction in the elongation values of CH films when combined with HPMC at 50% w/w (Tejada et al., 2017a). It is worth mentioning that high concentrations of plasticizers combined with CH as a polymer former could increase the elongation value, producing a decrease in the tensile strength (Domjan et al., 2009); however, load at break values (Figure 1C) ranged from 9 to 11 N with no significant differences among them ($p > 0.01$). The characteristics of films, based on biopolymers depend on an equilibrium between the degree of interactions in the polymeric matrix (which may induce brittleness), and the addition of plasticizers for better workability. It has been reported that above a critical concentration, the plasticizer can exceed the compatibility limit with the biopolymer, and phase separation with plasticizer exclusion is usually observed (Vieira et al., 2011). In this work the combinations of CH, HPMC, and PEG 400 at the assayed concentrations produced neither brittleness nor phase separation.

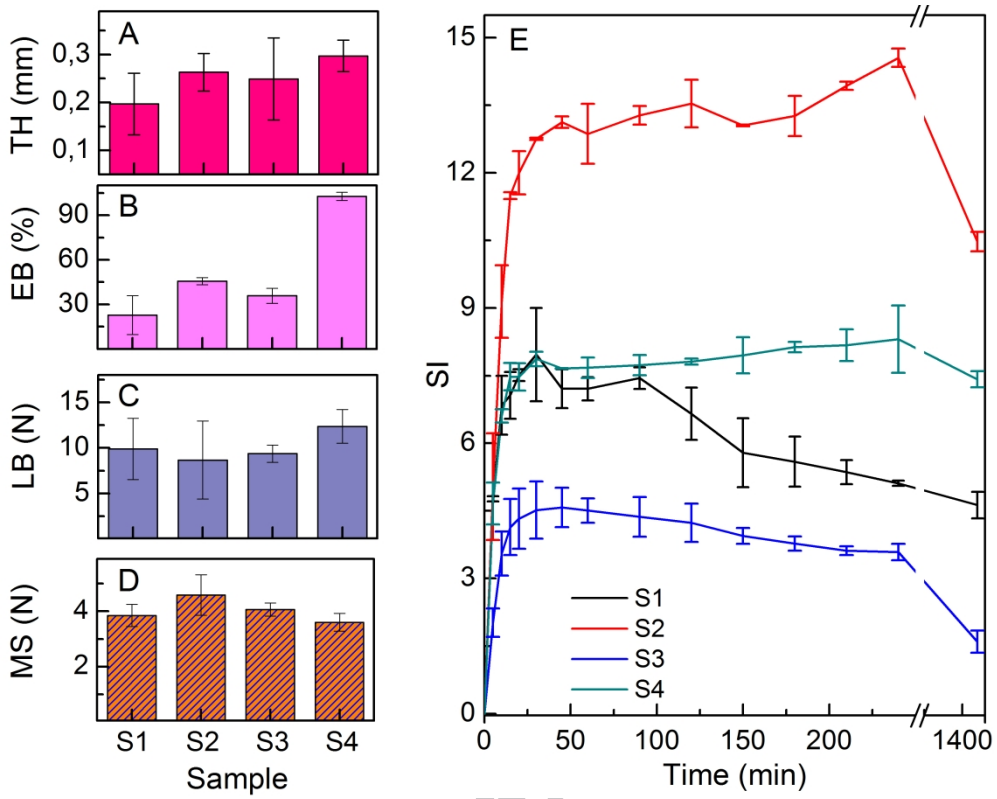

330

331

332 **Figure 1.** A) Thickness, B) Elongation at break C) Load at break D) Mucoadhesive strength

333 E) Sweeling index

334

335 3.2. Films swelling and adhesiveness

336 Figure 1E shows that films based only on CH (S2 and S4) swelled more than CH-

337 HPMC films (S1 and S3), this fact could be related with the pH value of the simulated

338 vaginal fluid (pH=4.2). At this pH value, CH is protonated (Dey et al., 2018; Wang et al.,

339 2006); thus, the more CH, the more charges, so there is more interaction with simulated

340 vaginal fluid and more fluid retention. The presence of HPMC in the formulated films did

341 not improve the swelling process due to the fact that high concentrations of HMPC could

342 decrease water permeability. Additionally, different results of the swelling process could

343 be due to the presence of the plastizicer. Conzatti et al. clearly described a CH

344 formulation film, employing high PEG 400 concentrations as a plastizicer, observing

PEG-PEG interactions instead of PEG-CH interactions (Conzatti et al., 2018). Consequently, a more organized, rigid structure was obtained, and thus the swelling could decrease. This phenomenon is observed in Figure 1E. Formulation S2 presented maximum swelling values, followed by formulation S4. The presence of high concentrations of CH improved water uptake, but the inclusion of a high concentration of plasticizer (40%), generated the opposite effect. A similar analysis was done observing Figure 1E, samples S3 and S1. Mucoadhesive strength results showed no significant differences among the formulated films ($p > 0.01$). Several works reported that as the swelling index increases the adhesive strength decreases. This fact is attributed to overhydration of the polymers that led to disentanglement at the polymers/tissue interface, resulting in an abrupt drop in adhesive strength (Bassi and Kaur, 2015; Peh and Wong, 1999). Based on the obtained result, the swelling of S2, despite being the highest, is not enough to decrease the adhesiveness of this formulation in comparison with S1, S3 and S4 ($p > 0.01$).

3.3. Spectroscopy data

Figure 2 shows the infrared spectra obtained for TCZ, polymers, plasticizer, commercial ovule and films. The FTIR-ATR spectrum of TCZ (Figure 2Aa, Table 2) was in agreement with the reference of the standard TCZ (KBr discs) of BP 2010 (British Pharmacopeia Comission, 2010). The characteristic peaks corresponding to ν(C═N) of the imidazol group 1562.3 cm^{-1}, δ(C─H) 1464.0 cm^{-1}, ν(C=C) 1433.1 cm^{-1}, ν(C─N) 1278.8 cm^{-1}, ν(C─O─C) 1118.7 cm^{-1}, ν(C─S) 733.0 cm^{-1} and ν(C─Cl) 626.9 cm^{-1} were identified (Bisht et al., 2015; Crisóstomo-Lucas et al., 2015).

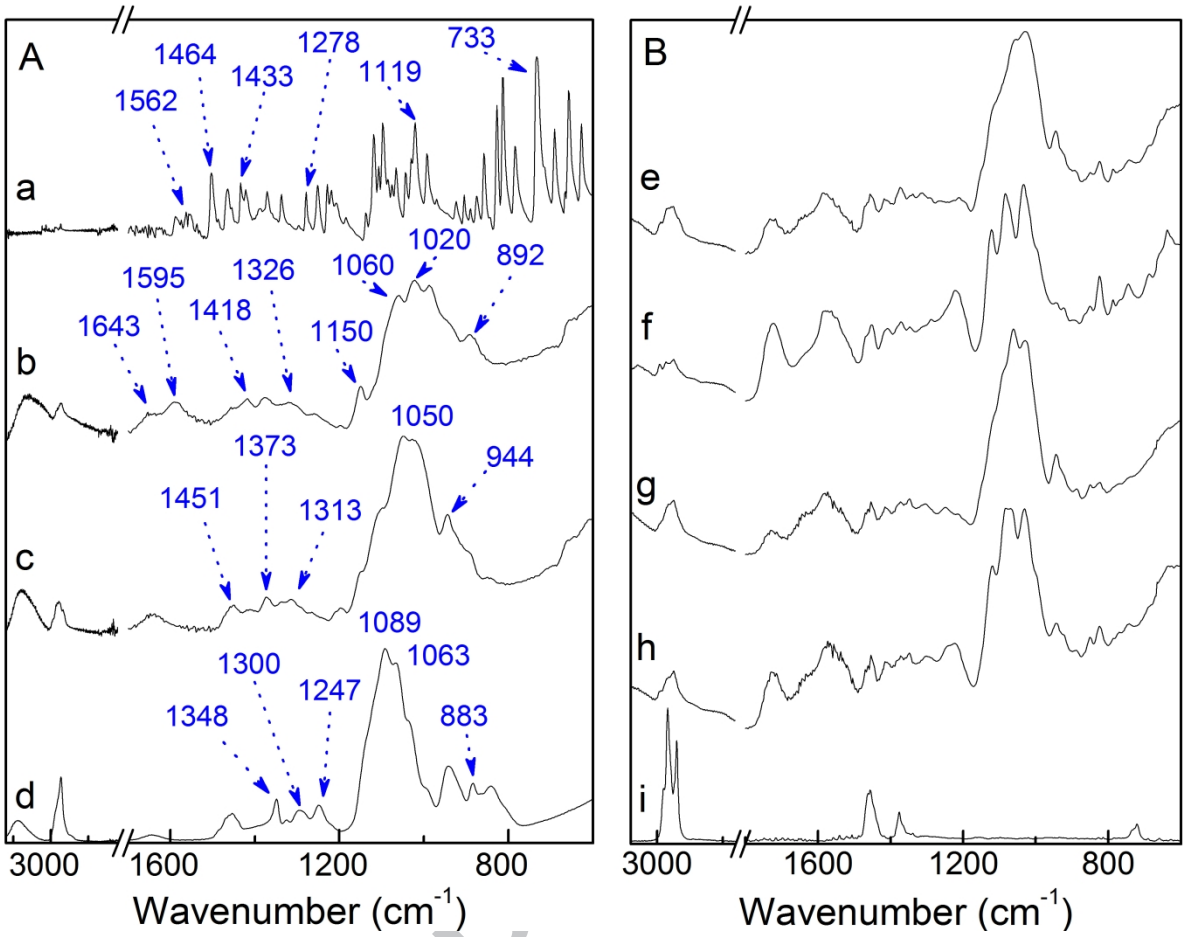

Figure 2. FTIR-ATR spectra. A) Components of films: a) TCZ, b) CH, c) HPMC d) PEG 400, B) Films and ovule: e) S1, f) S2, g) S3 h) S4 and i) Ovule.

The ATR-FTIR spectrum of CH (Figure 2Ab) showed a typical band between 3000-3600 cm^{-1}, concerned with –OH groups, which is broad due to overlapping with the stretching band of –NH (Pawlak and Mucha, 2003). Other bands were also observed centered at: 2925 cm^{-1} (stretching vibration of C─H bond); 1643cm^{-1} (amide I); 1595 cm^{-1} (NH_2 bending) (Tejada et al., 2017b); 1418 cm^{-1} (carboxyl –COOH) (Li et al., 2005); 1326 cm^{-1} (Amide III) (Kumar et al., 2017); 1150 cm^{-1} (stretching of the C–O–C bridge); 1060 cm^{-1} and 1020 cm^{-1} associated to the C–O stretching vibration (Espinosa-Andrews et al., 2010); and finally the band at 892 cm^{-1} assigned to the absorption peaks of β-(1,4) glycosidic unions in CH (Yue et al., 2009).

382 The HPMC spectrum (Figure 2Ac) in the region 3600-3200 cm^{-1} shows a band
383 associated with the presence of hydroxyl groups while the band in the region 3000-2800 cm^{-1}
384 represents the absorptions of C–H vibration modes from methyl group (Ding et al., 2015).
385 The band arising from –OH bonds on the glucose molecule appears at 1313 cm^{-1} and the
386 peaks at 1373 and 1451 cm^{-1} resulted from C─H bending and stretching modes from methyl
387 groups (Wang et al., 2007). The most intense peak in the HPMC spectrum occurred at
388 1050 cm^{-1} (C─O) and represents out-of-phase vibrations associated with an alkyl substituted
389 cyclic ring containing ether linkages (Akinosho et al., 2013). The peak centered at 944 cm^{-1}
390 represents the in-phase vibrations from ether linkages and appeared as a weaker band attached
391 to the band at 1050 cm^{-1} (Coates, 2000).

392 The spectrum of plasticizer (Figure 2Ad) PEG 400 presented a very intensive band
393 around 1100 cm^{-1} usually assigned in alcohols to either the ν(C–O) stretching or the in-plane
394 bending (δ) vibration of the C–O–H-group, and in ethers to the stretching ν(C–O–C)
395 vibration. The stretching ν(C–C) and deformational δ(–CH_2–) modes are also active in this
396 range (Rozenberg et al., 1998). The vibration band at 1300 cm^{-1} (antisymmetric stretch)
397 corresponds to the C–O–C ether stretch (Alcantar et al., 2000), while at 1348 cm^{-1} the (C–O–
398 H) deformational (in-plane) band appears (Rozenberg et al., 1998). The bands peaking at
399 2960 and 2869 cm^{-1} correspond to –CH_2 stretching vibrations (Alcantar et al., 2000).

400 The films (Figure 2Be-h) showed additional bands corresponding to lactic acid at 1727
401 cm^{-1} (C=O group); at 1220 cm^{-1} (O–H and C–O both from the acid group) and at 1120 cm^{-1}
402 (C–O alcohol group).

403 Several differences were observed when evaluating the IR spectra of the commercial
404 form and films (Figure 2B). The ovule (Figure 2Bi) presented only 7 bands, 4 of them may
405 correspond to TCZ (at 733 cm^{-1}, present in the spectrum as a shoulder; at 1338.6 cm^{-1}; at
406 1375.3 $cm^{-1}$and at 1456.5 cm^{-1}). In addition, the spectrum showed two bands comprised

between 2840 and 2950 cm^{-1} corresponding to C-H stretches of alkanes due to excipients of the ovule. The corresponding bands and assignments of the films developed are described in Table 2.

Table 2. FTIR-ATR spectroscopic data and assignment of the developed systems.

Wavenumber (cm^{-1})	S1	S2	S3	S4	Assignment
627*		+			TCZ
688	+	+			TCZ
743	+	+		Low intensity	TCZ
787	+	+		+	TCZ
883			+	+	PEG
945					HPMC
1120	+*	+		+	Lactic Acid
1220		+		+	Lactic Acid
1270-1315			+	+	PEG
1247			+	+*	PEG
1287		+			TCZ
1348		+	+	+	PEG
1727	+	+	+	+	Lactic Acid

* Signals corresponding to a shoulder

3.4. Thermal analysis

DSC curves show that TCZ exhibited a single endothermic peak (Figure 3A) without shoulders at 82.8 ºC, with an onset temperature of 77.6 ºC associated with the melting process (Ribeiro et al., 2016). This result is in agreement with the value reported (82 ºC) in the literature (British Pharmacopeia Comission, 2013). The calculated melting heat was 71.17 J/g and no re-crystallization peak was observed in the corresponding cooling curve. The thermogram of the commercial ovule (Figure 3B) shows an endothermic peak centered at 80.4 ºC, corresponding to the melting point of TCZ, which is slightly shifted to the right, probably due to some interactions with the excipients. Similar shifts were observed in previous works that studied drug-excipient compatibility. It was reported that these minor changes in the

melting endothermic peak of drug could be due to the mixing of drug and excipient, which lowers the purity of each component in the mixture and may not necessarily indicate potential incompatibility (Abrantes et al., 2016; Charde et al., 2008; Verma and Garg, 2005). On the other hand, no endothermic peak related with TCZ was observed in DSC analysis of the films (Figure 3C-F). The absence of the endothermic peak of TCZ could suggest that the drug is in amorphous state when loaded in the films (Rask et al., 2018; Senta-Loys et al., 2017).

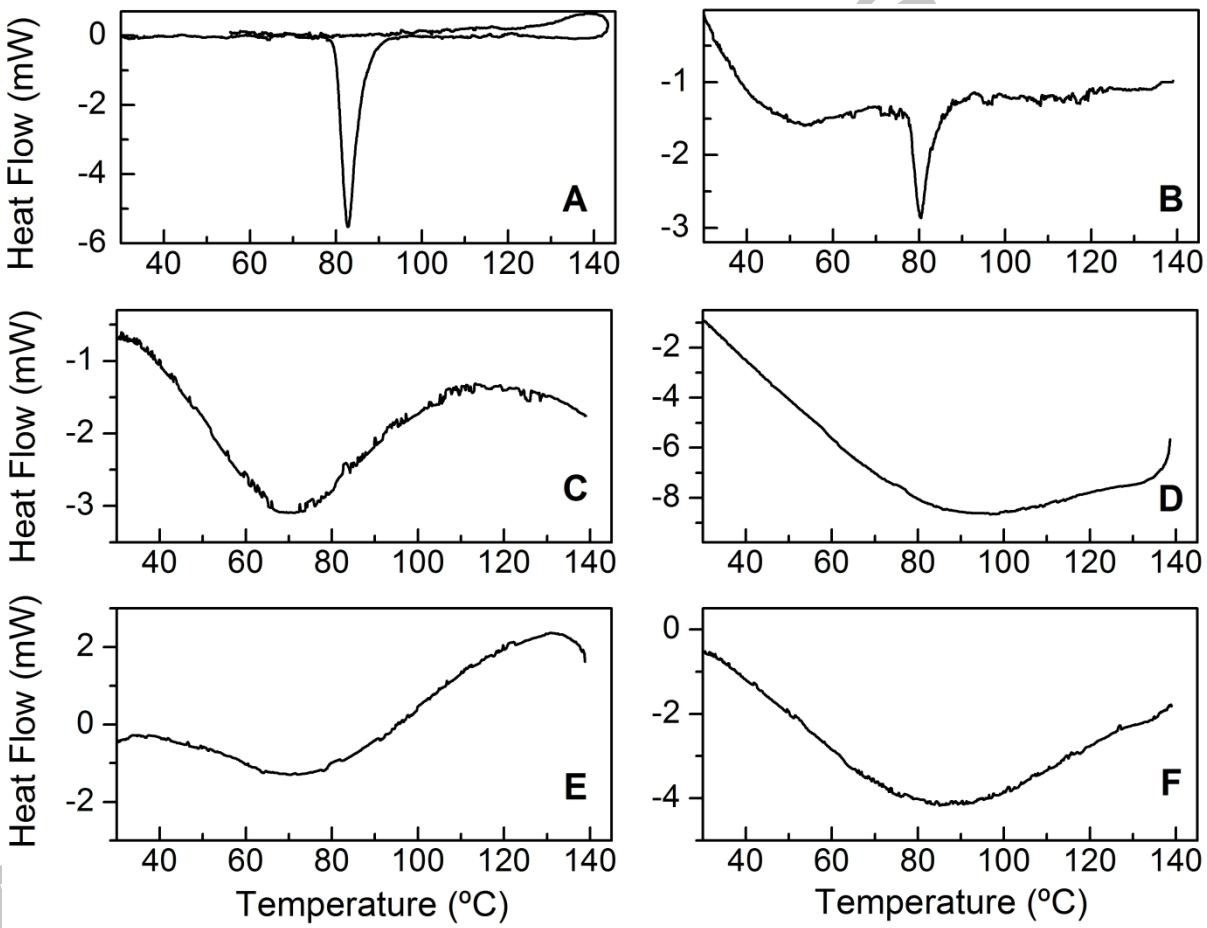

Figure 3. DSC thermograms. A) TCZ B) Ovule and C-F) films (S1, S2, S3, S4 respectively).

Regarding TGA (Table 4) and DTGA analysis, the commercial ovule exhibited 2 stages of degradation (Figure 4A), unlike TCZ whose degradation takes place in one stage (max peak 297.8 ºC Figure 4A). The greatest loss of mass (92.24%) in the decomposition of the

ovule took place between 30 and 360 ºC, with two maximum peaks of decomposition at 304.8 (related to TCZ) and 321.3 ºC (related to excipients).

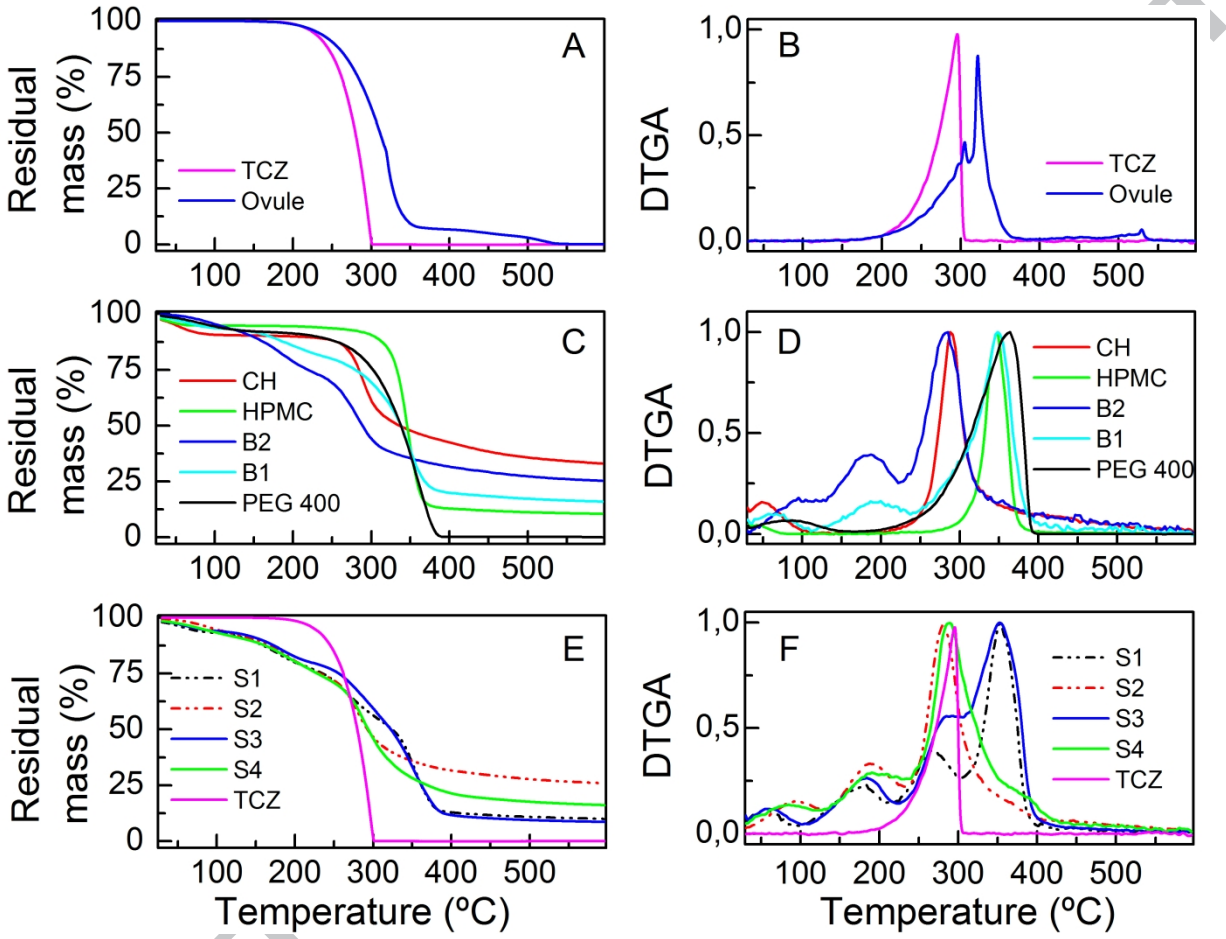

Figure 4. TGA and DTGA curves. A-B) TCZ and Ovule C-D) CH, HPMC, B2, B1, PEG 400 E-F) films S1, S2, S3, S4 and TCZ.

Figures 4C and 4D show that both polymers (HPMC and CH) in solid state showed 2 main degradation peaks, the first thermal event occurs in the temperature range 30-100 ºC and is attributed to the evaporation of water (de Britto and Campana-Filho, 2004). The second one occurs in the temperature range 200-400 ºC, and it is attributed to the thermal degradation of each polymer (345.9 ºC for HPMC/ 289.6 ºC for CH respectively) (de Britto and Campana-Filho, 2004; Li et al., 1999).

Films B1 and B2 containing only the polymers showed some differences with respect to solid polymers (Figures 4C and 4D). In the case of B1, 4 peaks can be observed; the first at 59.1 ºC is due to free water; the second, centered at 191.9 °C could be associated with water retained by polar interactions (Lavorgna et al., 2010); the next one, centered at 311.6 °C, corresponds to the fusion of CH (de Britto and Campana-Filho, 2004) and the last one, centered at 349.1 °C, corresponds to the fusion of HPMC (Li et al., 1999). B2 exhibited 3 peaks; one centered at 94.1 ° C associated to water linked through hydrogen bonds; another one at 179.5 ° C, which is related to water retained by polar interactions and finally the peak at 281.1 ° C, which is associated to the degradation of the polymer (Cardenas and Miranda, 2004).

The DTGA curve of the plasticizer exhibited three peaks (Figure 4 D); the first one centered at 81.2 ° C, is related to water linked through hydrogen bonds whereas the other two peaks, at 326.1 ° C and 362.7 ° C, correspond to the pyrolysis of PEG groups (Sadeghpour et al., 2018; Zhang et al., 2013).

The decomposition stages of the films can be observed in Figure 4E and 4F (Table 3). Whereas 3 stages are displayed for films based on CH, 4 stages were observed for films based on both polymers. For films S1 and S3, the first 2 peaks (52.7 and 171.1 ºC for S1 and 56.8 and 176.4 ºC for S3) have the same meaning as for B2, i.e. water volatilization; the third could be associated to simultaneous degradation of the drug and the CH (268.8 ºC for S1 and 289.2 ºC for S3), and the fourth peak is attributed to HPLC (353.5 and 353.1 ºC). S2 and S4 films exhibit only the first 3 peaks (Figure 4F) because these films do not contain HPMC in their composition. On the other hand, a decrease in the remaining mass was registered when the plasticizer concentration increased (Ramesh and Arof, 2001), independent of the polymer composition.

475 Table 3.TGA data.

	Remnant mass (%)	Stage 1 (ºC)	Peak (ºC)	Stage 2 (ºC)	Peak (ºC)	Stage 3 (ºC)	Peak (ºC)	Stage 4 (ºC)	Peak (ºC)
TCZ		180-307	297.8						
Ovule	-	30-360	304.8/321.3	360-550					
S1	9,98	25-100	52.70	100-215	171.02	215-304	268.78	304-425	353.54
S2	25,95	25-133	90.31	133-234	186.31	234-478	281.25		
S3	8,62	25-105	56.80	100-224	176.45	224-310	289.20	310-433	353.03
S4	16,06	25-123	81.57	123-240	185.95	240-478	292.39		

476

477 3.5. XRD analysis

478 The crystalline character of the drug was analyzed through an XRD analysis (Figure 5).
479 The TCZ raw material (Figure 5A) showed an intense peak at 22.33 º, which was mentioned
480 in a previous report (Ribeiro et al., 2016). Also, diffraction peaks at 2θ around 8.71 º; 10.39 º;
481 13.49 º; 13.67 º; 13.83 º; 16.35 º; 17.45 º; 17.93 º; 18.71 º; 20.33 º; 20.69 º; 24.01 º; 24.61 º;
482 25.33 º; 25.67 º; 26.27 º; 27.31 º; 27.53 º; 28.39 º; 28.99 º; 29.39 º; 29.83 º; 31.47 º; 32.17 º;
483 32.77 º; 33.13 º 36.95 º and 38.59 º were observed. The ovule (Figure 5B) showed 8 peaks
484 corresponding to the TCZ at 22.33 º, 27.31 º, 27.53 º, 28.39 º, 29.83 º, 31.47 º, 32.17 º and
485 33.13 º. Probably, the reduction in the intensities of the peaks regarding TCZ raw material is
486 due to the excipient dilution effect. On the other hand, no peaks were observed when
487 analyzing the spectra of the films (Figure 5 C-F), which is in agreement with the results
488 obtained by DSC, confirming the hypothesis that TCZ is in amorphous state inside the films
489 (Yang et al., 2018).

490

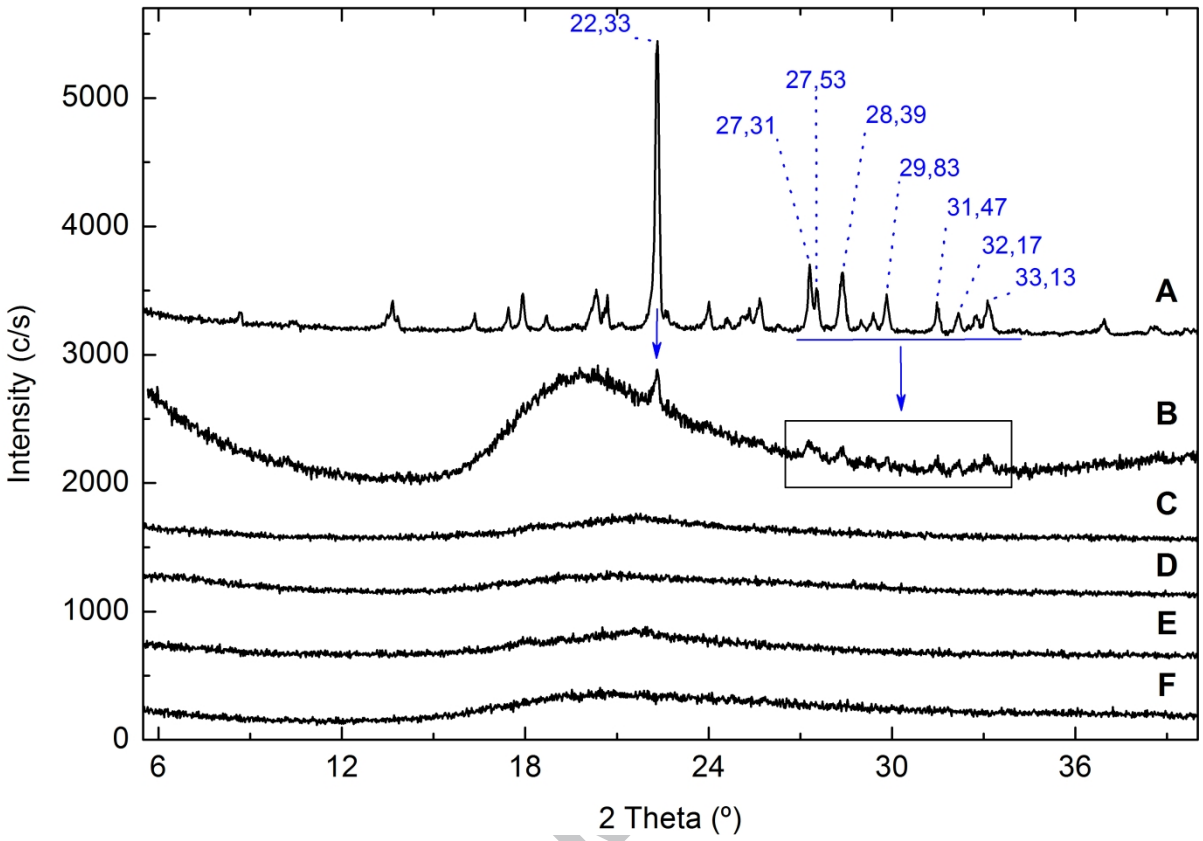

Figure 5. XRD pattern. A) TCZ B) Ovule C) S1 D) S2 E) S3 F) S4

3.6. SEM analysis

Morphology of films was analyzed by SEM (Figure 6). Figure 6A-D shows the SEM images of the surface and cross-sectional fracture of the films studied. The morphology of the films shows that all formulations were symmetric and uniformly distributed. In superficial section, film S1 based on CH-HPMC with 5% w/w PEG 400 (Figure 6A-A_2) presented a homogeneous and smooth surface even at 5000x magnification, while film S3 based on CH-HPMC with 40% w/w PEG 400 presented a few signs of roughness at 5000x (Figure $6C_2$) which may be attributed to the increase in the plasticizer content. On the other hand, films based only on CH (S2 and S4) showed to be porous and presented roughness at higher magnifications (Figure $6B_3$ and D_3), which could be related to the interaction between CH and

the plasticizer during the drying process (Al-Hassan and Norziah, 2012). As observed, the roughness increased in films containing 40% w/w PEG 400 (Figure 6C_2 and D_2).

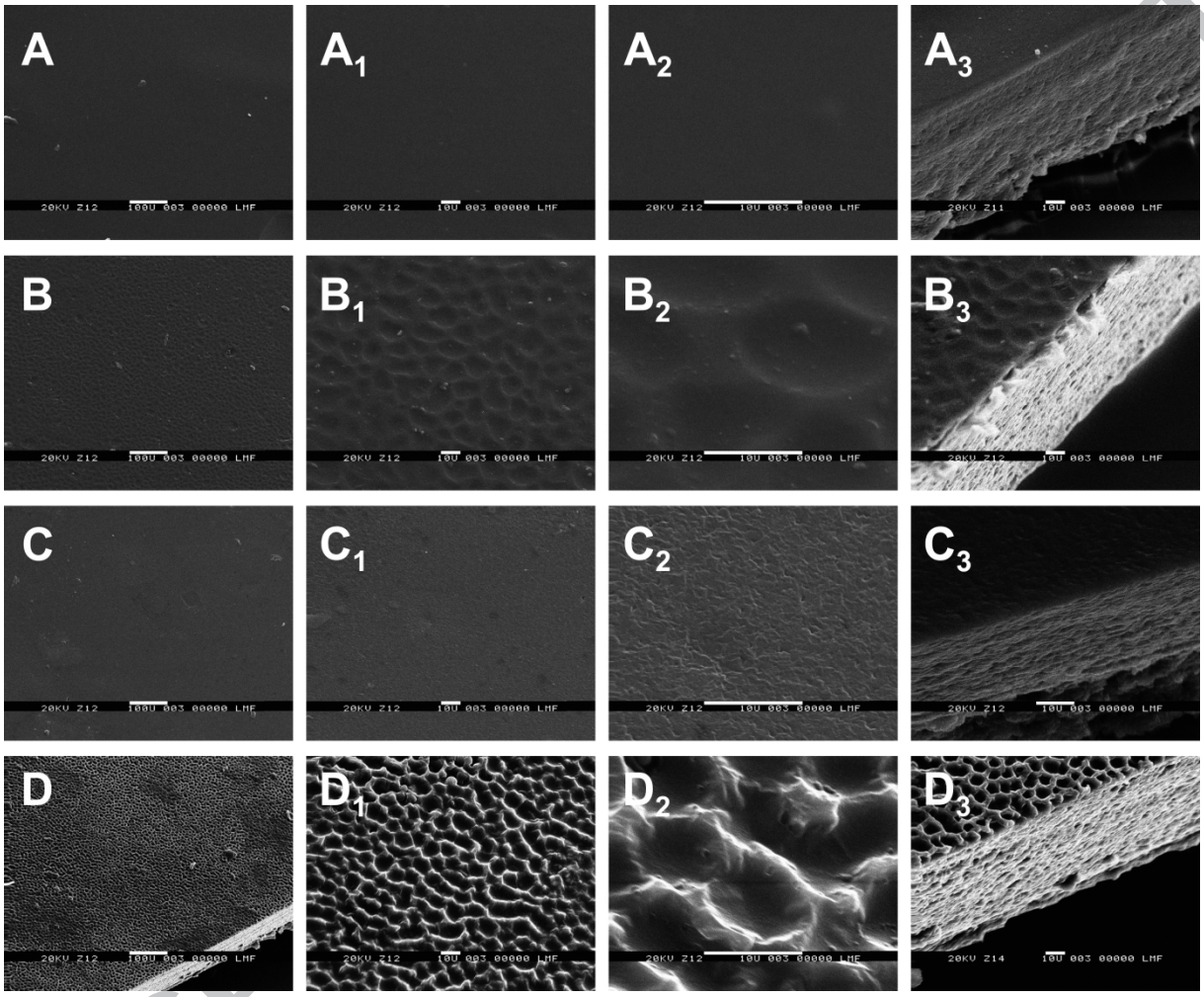

Figure 6. Scanning electron microscopy. A) S1 B) S2 (C) S3 (D) S4. Micrographs with different magnifications and orientation. Surface: A_D) 200x A_1_D_1) 1000x A_2_D_2) 5000x and film transversal section B_3_D_3)1000x.

It is important to remark that films based on CH and HPMC (Figure 6A and 6C) presented a dense and compact structure, suggesting high structural integrity and good compatibility between the components (Villacrés et al., 2014).

3.7. Dissolution Studies

Figure 7 shows the dissolution profiles of TCZ raw material and films. The films showed fast drug release, reaching almost 100% after 60 min (Figure 7). At 30 min assay, only 3.9 % of TCZ raw material was released (Q_{30}=3.9 %), while the films allowed a significant improvement in TCZ dissolution rate (S1 Q_{30} = 96.0 %, S2 Q_{30} = 88.2 %, S3 Q_{30}= 97.5 %, and S4 Q_{30}=83.5 %). The result is probably due to the fact that TZC modified its solid state when loaded in the films, as observed in DSC and XRD analysis. On the other hand, TCZ raw material presented incomplete dissolution after 360 min assay (Q_{360}=14.6 %). This poor dissolution is related to the TCZ structure, which is highly hydrophobic, belonging in class II in the Biopharmaceutical classification system (BCS) (Kasim et al., 2004).

This assay is useful for the analysis of TCZ release from the films; however, the assay conditions are not representative of the vaginal cavity, which presents humidity instead of 900 mL of fluid. To study TCZ release as well as its activity over time in a humid medium, the "halo zone test over time" was carried out.

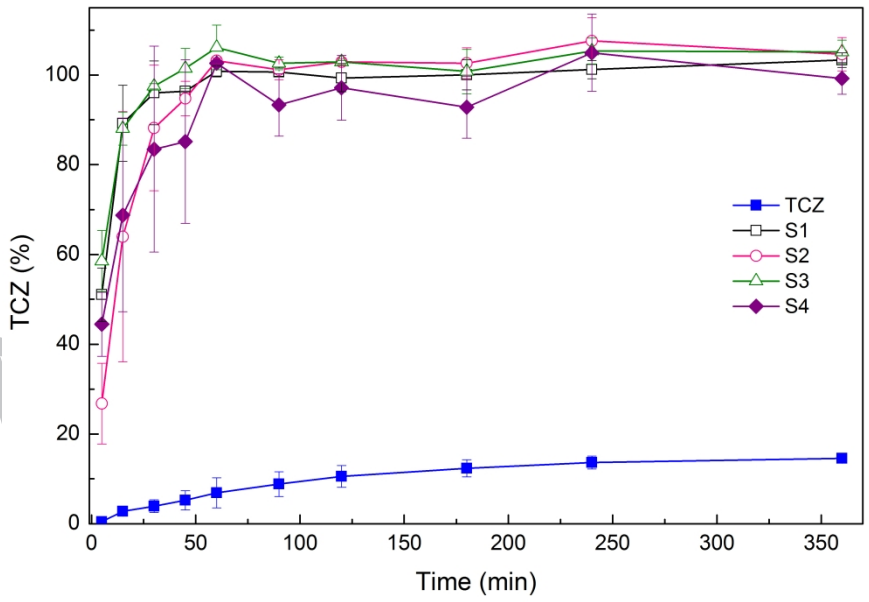

Figure 7. Dissolution profiles of TCZ and the films loaded with TCZ.

534 3.8. Biological activity

535 3.8.1. Halo zone test over time

536 Halo zone test over time was performed in order to analyze both the release of TCZ and
537 the activity of different formulations over time when exposed to a humid zone. Figure 8
538 shows the different halos produced over time by TZC raw material (added to a Scotch tape
539 disc), ovule content (embedded in a disc of absorbent paper), different film formulations, and
540 empty films (B1 and B2). As observed B2 based on 100% CH showed activity for 48 h, while
541 no inhibition halo was observed when B1 (based on CH:HPMC) was assayed. The ovule
542 presented antifungal activity until the end of the assay (5 mm). Films loaded with TZC
543 showed greater activity than both the ovule and TCZ raw material, producing inhibition halos
544 between 26-34 mm of diameters after 96 h assay. After 96 h, the percentage of reduction in
545 the diameter of the halo for the ovule in comparison with the first determination (2 h) was
546 89%, while the films showed reductions between 24 and 41% (S1= 35 % S2= 24 % S3= 38 %
547 S4= 41 %), suggesting a more time-sustained release of TCZ for the films.

548 No differences were observed between the behavior of the S3 and S4 formulations at the
549 end of the assay. On the other hand, S2 film (based on 100% CH and 5% PEG 400) produced
550 the highest inhibition halo at 24, 48, 72, and 96 h ($p < 0.01$); this result could be related with
551 both the swelling (Figure 1E) of the formulation (related with the highest release of TCZ from
552 the matrix to the culture medium) (Shu et al., 2001) and the activity of CH (observed in B2).

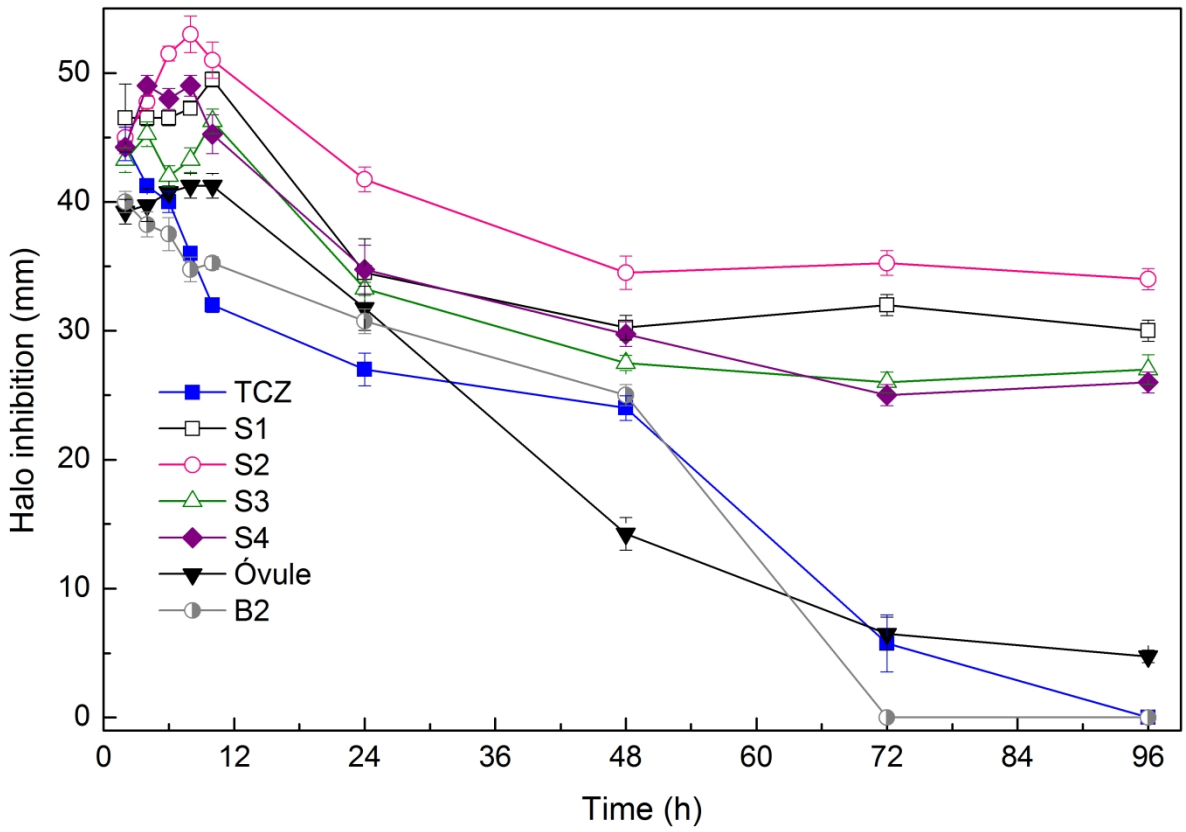

553

554 **Figure 8.** Halo zone produced by TCZ, films (S1-S4 and B2) and the commercial ovule.

555

556 3.8.2. Time-kill

557 Time-kill studies were performed to assess the exposure time required to kill a
558 standardized *Candida* inoculum. Plots of TCZ activity were built as CFU/mL versus time
559 (Figure 9). Times to obtain 99.9% reduction in the number of CFU/mL were different for each
560 formulation. It was observed that the control curve did not show any decrease in the number
561 of colony forming units compared with the initial inoculums, while a reduction in CFU was
562 observed even when unloaded film only containing CH was assayed. It has been reported that
563 low concentrations of CH produce a series of alterations of ion homeostasis and metabolism
564 of the yeast while at high concentrations it may act as a permeation agent for bacteria and
565 fungi (Peña et al., 2013). Thus, when CH is used at concentrations higher than 1.0 mg/mL, not
566 only a fungistatic but also a fungicidal activity is observed. In this assay the CH concentration

(when placing unloaded film based only on CH into the medium) was higher than 1.0 mg/mL, therefore, this unloaded film (B2) presented fungicidal activity itself. On the other hand, when CH was used at 25% (B1) the concentration in the medium was lower than 1.0 mg/mL and no decrease in the number of colony forming units compared with the initial inoculums was observed.

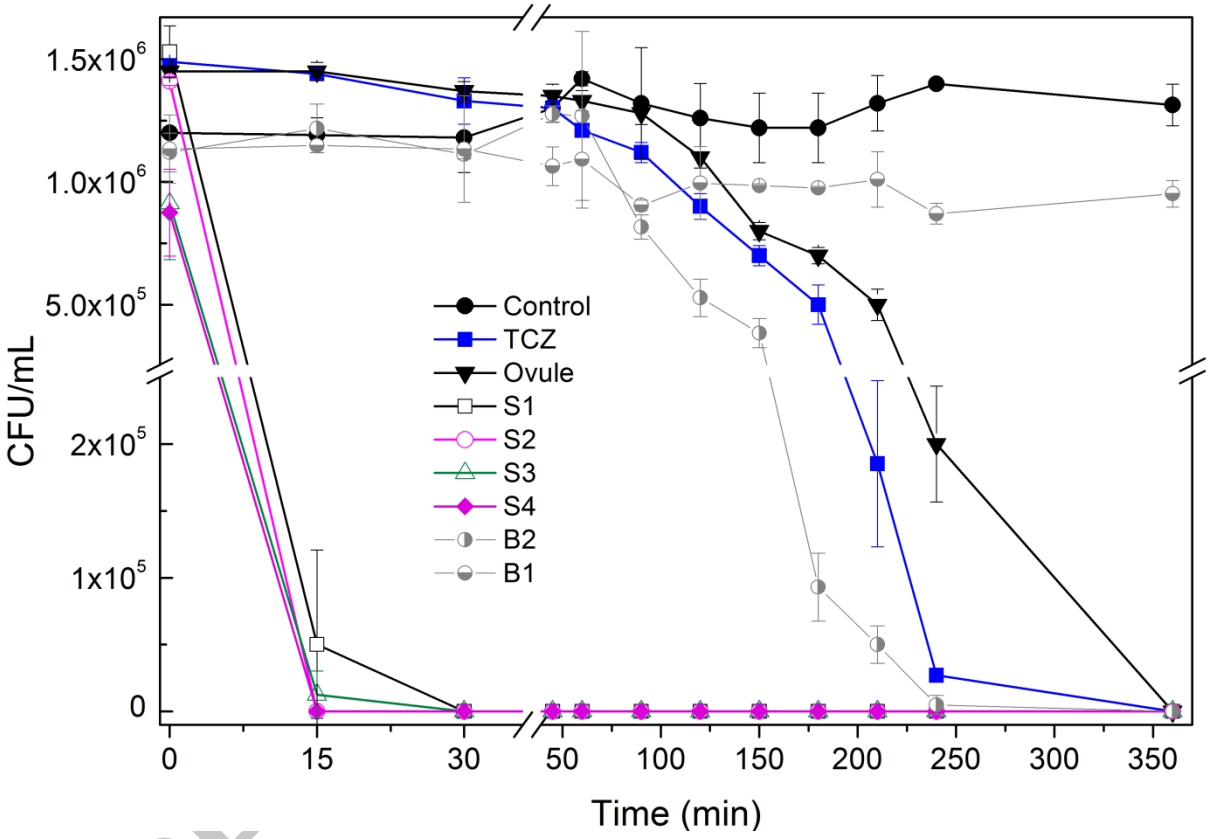

Figure 9. CFU/mL surviving at each time point in the presence and absence of the different formulations.

When TCZ was loaded, the activity of the formulations was directly related to the drug, and just small differences between time-kill curves of loaded films (S1-S4) were found (Figure 9). The fastest activity was obtained when loaded CH (15 minutes) or CH-HPMC (30 minutes) based films were assayed; on the other hand, both TCZ raw material and the ovule needed 360 minutes to reach this reduction. This was probably related to the higher and faster dissolution of TCZ when it is loaded in the films (Figure 7), which may improve its diffusion

582 in the agar medium. This increase in TCZ diffusion may explain the higher activity of the
583 films with respect to TCZ pure drug and ovule.

584

585 3.9. Cytotoxicity of loaded and unloaded films

586 Regarding cytotoxicity (Figure 10), films only based on CH induced a 35 to 54 % reduction in
587 cell viability after 24 h incubation, as compared to control films. It has been reported that CH
588 seems to be cytostatic towards fibroblasts; due to the fact that it inhibits cell proliferation.
589 Thus, CH-based materials would alter cell growth; however, Shahabeddin et. al found that
590 combinations of CH with other materials, such as collagen and glycosaminoglycans, allow
591 improvement of its cytocompatibility (Shahabeddin et al., 1991). On the other hand, films
592 based on CH-HPMC (loaded and unloaded) did not produce any cytotoxicity effects.

593

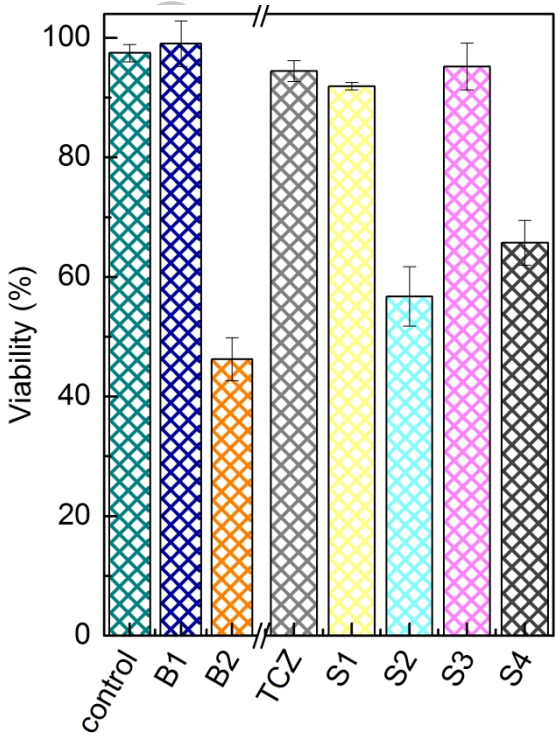

594

595 Figure 10. Cytotoxicity of loaded and unloaded films

596

3. Conclusions

In this work, vaginal films based on CH alone and combined with HPMC using different contents of PEG as plasticizer were successfully developed and characterized as an alternative dosage form for the treatment of vaginal candidiasis. Formulated films showed similar mechanical properties and adhesiveness. The films were able to swell for 24 h without suffering disintegration; however, films based only on CH showed the highest swelling and, therefore, may produce discomfort after application. The developed films displayed faster activity against *Candida albicans* than both TCZ pure drug and TCZ ovule, which is probably associated with the fact that TCZ is inside the films in amorphous state. Additionally, films presented controlled release of TCZ, showing strong antifungal activity after 96 h assay. Those formulations based only on CH presented a certain degree of cytotoxicity and, therefore, their use should be avoided. The system based on CH-HPMC with 40% PEG 400 as plasticizer showed fast and sustained antimicrobial activity and also the lowest swelling value. Additionally, this formulation produced no cytotoxic effects, showing that this film is a promising alternative dosage form for the treatment of vaginal candidiasis. All these tests should be supplemented by *in vivo* tests in the near future.

Acknowledgements

The authors gratefully acknowledge Consejo Nacional de Investigaciones Científicas y Técnicas (CONICET), Agencia Nacional de Promoción de Ciencia y Tecnología (ANPCyT), and Universidad Nacional de Rosario (UNR) for their financial support. NLC is also thankful to CONICET for her fellowship. ADQ thanks Carla G. Comanzo for technical assistance in cytotoxicity assays. In addition, we would like to thank the staff from the English Department (Facultad de Cs. Bioquímicas y Farmacéuticas, Universidad Nacional de Rosario) for the language correction of the manuscript.

Figure Captions

Figure 1. A) Thickness, B) Elongation at break C) Load at break D) Mucoadhesive strength E) Sweeling index

Figure 2. FTIR-ATR spectra. A) Components of films: a) TCZ, b) CH, c) HPMC d) PEG 400, B) Films and ovule: e) S1, f) S2, g) S3 h) S4 and i) Ovule

Figure 3. DSC thermograms. A) TCZ B) Ovule and C-F) films (S1, S2, S3, S4 respectively)

Figure 4. TGA and DTGA curves. A-B) TCZ and Ovule C-D) CH, HPMC, B2, B1, PEG 400 E-F) films S1, S2,S3,S4 and TCZ.

Figure 5. XRD pattern. A) TCZ B) Ovule C) S1 D) S2 E) S3 F) S4

Figure 6. Scanning electron microscopy. A) TCZ. B) S1 C) S2 (D) S3 (E) S4. Micrographs with different magnifications and orientation. Surface: A.F) 200x A_1-F_1) 1000x A_2-F_2) 5000x and film transversal section B_3-F_3)1000x

Figure 7. Dissolution profiles of TCZ and the films loaded with TCZ.

Figure 8. Inhibition halos produced by TCZ, films (S1-S4 and B2) and the commercial ovule.

Figure 9. CFU/mL surviving at each time point in the presence and absence of the different formulations.

Figure 10. Cytotoxicity of loaded and unloaded films

References

Abrantes, C.G., Duarte, D., Reis, C.P., 2016. An Overview of Pharmaceutical Excipients: Safe or Not Safe? Journal of Pharmaceutical Sciences 105, 2019-2026.

Akinosho, H., Hawkins, S., Wicker, L., 2013. Hydroxypropyl methylcellulose substituent analysis and rheological properties. Carbohydrate polymers 98, 276-281.

Al-Hassan, A.A., Norziah, M.H., 2012. Starch–gelatin edible films: Water vapor permeability and mechanical properties as affected by plasticizers. Food Hydrocolloids 26, 108-117.

Alam, M.A., Ahmad, F.J., Khan, Z.I., Khar, R.K., Ali, M., 2007. Development and evaluation of acid-buffering bioadhesive vaginal tablet for mixed vaginal infections. AAPS PharmSciTech 8, 229.

Alcantar, N.A., Aydil, E.S., Israelachvili, J.N., 2000. Polyethylene glycol-coated biocompatible surfaces. Journal of biomedical materials research 51, 343-351.

Allen, D.D., Caviedes, R., Cárdenas, A.M., Shimahara, T., Segura-Aguilar, J., Caviedes, P.A., 2005. Cell Lines as In Vitro Models for Drug Screening and Toxicity Studies. Drug Development and Industrial Pharmacy 31, 757-768.

654 Avachat, A.M., Gujar, K.N., Wagh, K.V., 2013. Development and evaluation of tamarind seed
655 xyloglucan-based mucoadhesive buccal films of rizatriptan benzoate. Carbohydrate polymers 91,
656 537-542.
657 Bassi, P., Kaur, G., 2015. Bioadhesive vaginal drug delivery of nystatin using a derivatized polymer:
658 development and characterization. European Journal of Pharmaceutics and Biopharmaceutics 96,
659 173-184.
660 Beggs, W.H., 1984. Fungicidal activity of tioconazole in relation to growth phase of Candida albicans
661 and Candida parapsilosis. Antimicrobial agents and chemotherapy 26, 699-701.
662 Bisht, D.S., Bhatt, G.K., Kothiyal, P., 2015. Formulation and Evaluation of Nail Lacquer Containing
663 Tioconazole for Transungual Drug Delivery System. Indo Am. J. Pharm. Sci. 2, 1474-1485.
664 British Pharmacopeia Comission, 2013. Tioconazole impurity standard.
665 British Pharmacopeia Comission, 2010. British Pharmacopeia, Londres.
666 Cantón, E., Pemán, J., Valentín, A., Espinel-Ingroff, A., Gobernado, M., 2009. In vitro activities of
667 echinocandins against Candida krusei determined by three methods: MIC and minimal fungicidal
668 concentration measurements and time-kill studies. Antimicrobial agents and chemotherapy 53,
669 3108-3111.
670 Cardenas, G., Miranda, S.P., 2004. FTIR and TGA studies of chitosan composite films. Journal of the
671 Chilean Chemical Society 49, 291-295.
672 Carrillo-Muñoz, A.J., Tur-Tur, C., Hernández-Molina, J.M., Santos, P., Cárdenes, D., Giusiano, G., 2010.
673 Antifúngicos disponibles para el tratamiento de las micosis ungueales. Revista iberoamericana de
674 micologia 27, 49-56.
675 Cautela, M.P., Moshe, H., Sosnik, A., Sarmento, B., das Neves, J., 2018. Composite films for vaginal
676 delivery of tenofovir disoproxil fumarate and emtricitabine. European Journal of Pharmaceutics and
677 Biopharmaceutics.
678 Coates, J., 2000. Interpretation of infrared spectra, a practical approach. Encyclopedia of analytical
679 chemistry.
680 Conzatti, G., Chamary, S., De Geyter, N., Cavalie, S., Morent, R., Tourrette, A., 2018. Surface
681 functionalization of plasticized chitosan films through PNIPAM grafting via UV and plasma graft
682 polymerization. European Polymer Journal.
683 Costa-de-Oliveira, S., Pina-Vaz, C., Mendonca, D., Rodrigues, A.G., 2008. A first Portuguese
684 epidemiological survey of fungaemia in a university hospital. European Journal of Clinical
685 Microbiology & Infectious Diseases 27, 365-374.
686 Crisóstomo-Lucas, C., García-Holley, P., Hernández-Ortega, S., Sánchez-Bartéz, F., Gracia-Mora, I.,
687 Barba-Behrens, N., 2015. Structural characterization and cytotoxic activity of tioconazole
688 coordination compounds with cobalt(II), copper(II), zinc(II) and cadmium(II). Inorganica Chimica Acta
689 438, 245-254.
690 Charde, S., Mudgal, M., Kumar, L., Saha, R., 2008. Development and evaluation of buccoadhesive
691 controlled release tablets of lercanidipine. AAPS PharmSciTech 9, 182-190.
692 de Britto, D., Campana-Filho, S.P., 2004. A kinetic study on the thermal degradation of N,N,N-
693 trimethylchitosan. Polymer Degradation and Stability 84, 353-361.
694 Dey, A., Kamat, A., Nayak, S., Danino, D., Kesselman, E., Dandekar, P., Jain, R., 2018. Role of proton
695 balance in formation of self-assembled chitosan nanoparticles. Colloids and Surfaces B: Biointerfaces
696 166, 127-134.
697 Ding, C., Zhang, M., Li, G., 2015. Preparation and characterization of collagen/hydroxypropyl
698 methylcellulose (HPMC) blend film. Carbohydrate Polymers 119, 194-201.
699 Dobaria, N.B., Badhan, A., Mashru, R., 2009. A novel itraconazole bioadhesive film for vaginal
700 delivery: design, optimization, and physicodynamic characterization. Aaps Pharmscitech 10, 951.
701 Domjan, A., Bajdik, J., Pintye-Hodi, K., 2009. Understanding of the plasticizing effects of glycerol and
702 PEG 400 on chitosan films using solid-state NMR spectroscopy. Macromolecules 42, 4667-4673.
703 Egan, M.E., Lipsky, M.S., 2000. Diagnosis of vaginitis. American family physician 62, 1095-1104.

704 Espinosa-Andrews, H., Sandoval-Castilla, O., Vázquez-Torres, H., Vernon-Carter, E.J., Lobato-Calleros,
705 C., 2010. Determination of the gum Arabic–chitosan interactions by Fourier Transform Infrared
706 Spectroscopy and characterization of the microstructure and rheological features of their
707 coacervates. Carbohydrate Polymers 79, 541-546.
708 Ferretti, A.C., Tonucci, F.M., Hidalgo, F., Almada, E., Larocca, M.C., Favre, C., 2016. AMPK and PKA
709 interaction in the regulation of survival of liver cancer cells subjected to glucose starvation.
710 Oncotarget 7, 17815-17828.
711 Ghosal, K., Ranjan, A., Bhowmik, B.B., 2014. A novel vaginal drug delivery system: anti-HIV
712 bioadhesive film containing abacavir. Journal of Materials Science: Materials in Medicine 25, 1679-
713 1689.
714 Kamel, S., Ali, N., Jahangir, K., Shah, S., El-Gendy, A., 2008. Pharmaceutical significance of cellulose: a
715 review. Express Polym Lett 2, 758-778.
716 Kasim, N.A., Whitehouse, M., Ramachandran, C., Bermejo, M., Lennernäs, H., Hussain, A.S.,
717 Junginger, H.E., Stavchansky, S.A., Midha, K.K., Shah, V.P., Amidon, G.L., 2004. Molecular Properties
718 of WHO Essential Drugs and Provisional Biopharmaceutical Classification. Molecular Pharmaceutics 1,
719 85-96.
720 Krajewska, B., 2004. Application of chitin-and chitosan-based materials for enzyme immobilizations: a
721 review. Enzyme and microbial technology 35, 126-139.
722 Kumar, N., Devineni, S.R., Gajjala, P.R., Dubey, S.K., Kumar, P., 2017. Synthesis, isolation,
723 identification and characterization of new process-related impurity in isoproterenol hydrochloride by
724 HPLC, LC/ESI-MS and NMR. J. Pharm. Anal. 7, 394-400.
725 Lavorgna, M., Piscitelli, F., Mangiacapra, P., Buonocore, G.G., 2010. Study of the combined effect of
726 both clay and glycerol plasticizer on the properties of chitosan films. Carbohydrate Polymers 82, 291-
727 298.
728 Lefler, E., Stevens, D.A., 1984. Inhibition and killing of Candida albicans in vitro by five imidazoles in
729 clinical use. Antimicrobial agents and chemotherapy 25, 450-454.
730 Li, X.-G., Huang, M.-R., Bai, H., 1999. Thermal decomposition of cellulose ethers. Journal of Applied
731 Polymer Science 73, 2927-2936.
732 Li, Z., Ramay, H.R., Hauch, K.D., Xiao, D., Zhang, M., 2005. Chitosan–alginate hybrid scaffolds for bone
733 tissue engineering. Biomaterials 26, 3919-3928.
734 Machado, A., Cunha-Reis, C., Araújo, F., Nunes, R., Seabra, V., Ferreira, D., das Neves, J., Sarmento,
735 B., 2016. Development and in vivo safety assessment of tenofovir-loaded nanoparticles-in-film as a
736 novel vaginal microbicide delivery system. Acta biomaterialia 44, 332-340.
737 Mishra, R., Soni, K., Mehta, T., 2017. Mucoadhesive vaginal film of fluconazole using cross-linked
738 chitosan and pectin. Journal of Thermal Analysis and Calorimetry 130, 1683-1695.
739 Owen, D.H., Katz, D.F., 1999. A vaginal fluid simulant. Contraception 59, 91-95.
740 Pawlak, A., Mucha, M., 2003. Thermogravimetric and FTIR studies of chitosan blends. Thermochimica
741 acta 396, 153-166.
742 Peh, K.K., Wong, C.F., 1999. Polymeric films as vehicle for buccal delivery: swelling, mechanical, and
743 bioadhesive properties. J Pharm Pharm Sci 2, 53-61.
744 Peña, A., Sánchez, N.S., Calahorra, M., 2013. Effects of chitosan on Candida albicans: conditions for
745 its antifungal activity. BioMed research international 2013.
746 Pharmacopoeia, U., 2017. USP 40, NF 35, Pharmacopoeia, US -National Formulary. Rockville: USP 2.
747 Priotti, J., Codina, A.V., Leonardi, D., Vasconi, M.D., Hinrichsen, L.I., Lamas, M.C., 2017. Albendazole
748 microcrystal formulations based on chitosan and cellulose derivatives: physicochemical
749 characterization and in vitro parasiticidal activity in Trichinella spiralis adult worms. AAPS
750 PharmSciTech 18, 947-956.
751 Ramesh, S., Arof, A.K., 2001. Structural, thermal and electrochemical cell characteristics of poly(vinyl
752 chloride)-based polymer electrolytes. Journal of Power Sources 99, 41-47.
753 Rask, M.B., Knopp, M.M., Olesen, N.E., Holm, R., Rades, T., 2018. Comparison of two DSC-based
754 methods to predict drug-polymer solubility. International Journal of Pharmaceutics 540, 98-105.

Ribeiro, R.F., Motta, M.H., Härter, A.P.G., Flores, F.C., Beck, R.C.R., Schaffazick, S.R., da Silva, C.d.B., 2016. Spray-dried powders improve the controlled release of antifungal tioconazole-loaded polymeric nanocapsules compared to with lyophilized products. Materials Science and Engineering: C 59, 875-884.

Rozenberg, M., Loewenschuss, A., Marcus, Y., 1998. IR spectra and hydration of short-chain polyethyleneglycols. Spectrochimica Acta Part A: Molecular and Biomolecular Spectroscopy 54, 1819-1826.

Sadeghpour, M., Yusoff, R., Aroua, M.K., Tabandeh, M., 2018. Modification of polyethylene glycol with choline chloride and evaluation of the CO2 absorption capacity of their aqueous solutions. Greenhouse Gases: Science and Technology 8, 324-334.

Saha, D., Bhattacharya, S., 2010. Hydrocolloids as thickening and gelling agents in food: a critical review. Journal of food science and technology 47, 587-597.

Senta-Loys, Z., Bourgeois, S., Valour, J.-P., Briançon, S., Fessi, H., 2017. Orodispersible films based on amorphous solid dispersions of tetrabenazine. International Journal of Pharmaceutics 518, 242-252.

Shahabeddin, L., Damour, O., Berthod, F., Rousselle, P., Saintigny, G., Collombel, C., 1991. Reconstructed skin from co-cultured human keratinocytes and fibroblasts on a chitosane cross-linked collagen-GAG matrix. Journal of Materials Science: Materials in Medicine 2, 222-226.

Shaker, D.S., Ismail, S., Hamed, S., El-Shishtawy, E.M., 2018. Butoconazole nitrate vaginal sponge: Drug release and antifungal efficacy. Journal of Drug Delivery Science and Technology 48, 274-287.

Shu, X., Zhu, K., Song, W., 2001. Novel pH-sensitive citrate cross-linked chitosan film for drug controlled release. International journal of pharmaceutics 212, 19-28.

Srinivasan, P., Zhang, J., Martin, A., Kelley, K., McNicholl, J.M., Buckheit, R.W., Smith, J.M., Ham, A.S., 2016. Safety and pharmacokinetics of quick-dissolving polymeric vaginal films delivering the antiretroviral IQP-0528 for preexposure prophylaxis. Antimicrobial agents and chemotherapy 60, 4140-4150.

Suyatma, N.E., Tighzert, L., Copinet, A., Coma, V., 2005. Effects of hydrophilic plasticizers on mechanical, thermal, and surface properties of chitosan films. Journal of Agricultural and Food Chemistry 53, 3950-3957.

Tejada, G., Barrera, M., Piccirilli, G., Sortino, M., Frattini, A., Salomón, C., Lamas, M.C., Leonardi, D., 2017a. Development and evaluation of buccal films based on chitosan for the potential treatment of oral candidiasis. AAPS PharmSciTech 18, 936-946.

Tejada, G., Lamas, M., Sortino, M., Alvarez, V., Leonardi, D., 2018a. Composite Microparticles Based on Natural Mucoadhesive Polymers with Promising Structural Properties to Protect and Improve the Antifungal Activity of Miconazole Nitrate. AAPS PharmSciTech, 1-11.

Tejada, G., Lamas, M.C., Svetaz, L., Salomón, C.J., Alvarez, V.A., Leonardi, D., 2018b. Effect of drug incorporation technique and polymer combination on the performance of biopolymeric antifungal buccal films. International Journal of Pharmaceutics 548, 431-442.

Tejada, G., Piccirilli, G., Sortino, M., Salomón, C., Lamas, M., Leonardi, D., 2017b. Formulation and in-vitro efficacy of antifungal mucoadhesive polymeric matrices for the delivery of miconazole nitrate. Materials Science and Engineering: C 79, 140-150.

Traore, Y.L., Fumakia, M., Gu, J., Ho, E.A., 2018. Dynamic mechanical behaviour of nanoparticle loaded biodegradable PVA films for vaginal drug delivery. Journal of biomaterials applications 32, 1119-1126.

Verma, R.K., Garg, S., 2005. Selection of excipients for extended release formulations of glipizide through drug–excipient compatibility testing. Journal of pharmaceutical and biomedical analysis 38, 633-644.

Vieira, M.G.A., da Silva, M.A., dos Santos, L.O., Beppu, M.M., 2011. Natural-based plasticizers and biopolymer films: A review. European Polymer Journal 47, 254-263.

Villacrés, R.A.E., Flores, S.K., Gerschenson, L.N., 2014. Biopolymeric antimicrobial films: study of the influence of hydroxypropyl methylcellulose, tapioca starch and glycerol contents on physical properties. Materials Science and Engineering: C 36, 108-117.

Wang, L., Dong, W., Xu, Y., 2007. Synthesis and characterization of hydroxypropyl methylcellulose and ethyl acrylate graft copolymers. Carbohydrate Polymers 68, 626-636.
Wang, Q.Z., Chen, X.G., Liu, N., Wang, S.X., Liu, C.S., Meng, X.H., Liu, C.G., 2006. Protonation constants of chitosan with different molecular weight and degree of deacetylation. Carbohydrate Polymers 65, 194-201.
Yang, J., Alvebratt, C., Lu, X., Bergström, C.A.S., Strømme, M., Welch, K., 2018. Amorphous magnesium carbonate nanoparticles with strong stabilizing capability for amorphous ibuprofen. International Journal of Pharmaceutics 548, 515-521.
Yoo, J.-W., Acharya, G., Lee, C.H., 2009. In vivo evaluation of vaginal films for mucosal delivery of nitric oxide. Biomaterials 30, 3978-3985.
Yue, W., He, R., Yao, P., Wei, Y., 2009. Ultraviolet radiation-induced accelerated degradation of chitosan by ozone treatment. Carbohydrate Polymers 77, 639-642.
Zhang, L., Wang, Z., Lu, Z., Shen, H., Huang, J., Zhao, Q., Liu, M., He, N., Zhang, Z., 2013. PEGylated reduced graphene oxide as a superior ssRNA delivery system. Journal of Materials Chemistry B 1, 749-755.